Three Leg Inverter Control based on Laguerre Model Predictive Controller

Adelhard Beni Rehiara
Department of Electrical Engineering, University of Papua, Indonesia
a.rehiara@unipa.ac.id (corresponding author)

Yanty Rumengan
Department of Electrical Engineering, University of Papua, Indonesia
y.rumengan@unipa.ac.id

Pandung Sarungallo
Department of Electrical Engineering, University of Papua, Indonesia
p.sarungallo@unipa.ac.id

Hendri
Department of Forestry, University of Papua, Indonesia
h.hendri@unipa.ac.id

Received: 13 July 2024 | Revised: 23 August 2024 | Accepted: 3 September 2024

 DOI: https://doi.org/10.48084/etasr.8385

ABSTRACT

An inverter is a power electronic device that converts Direct Current (DC) to Alternating Current (AC). A three-leg inverter was used to convert DC to AC in a three-phase form. The increasing need to integrate renewable energy into the power grid has increased the demand for this type of converter. In this paper, a Laguerre-based Model Predictive Controller (LMPC) is proposed to control a three-leg inverter under load variation. The proposed LMPC algorithm was designed to optimize the inverter performance and was compared with traditional Sinusoidal Pulse Width Modulation (SPWM) methods. Simulations were conducted under various load conditions including resistive (R), capacitive (RC), and induction motor loads. The results demonstrate that the LMPC controller outperforms the SPWM methods, providing better performance and lower Total Harmonic Distortion (THD) values. The THDs of the voltage and current achieved by the LMPC controller were below 1.5%, complying with IEEE 519-2014 standards. However, the current THD increased to 7.18% under the induction motor load.

Keywords-inverter; SPWM; Laguerre MPC; load variation; THD

I. INTRODUCTION

The development of new and renewable energy sources has made it possible for humans to use them as an alternative energy source in the future [1]. Alternative energies that are easy and inexpensive to apply without the need for complex infrastructure on a small scale are wind and solar power. These two types of energy are dynamic, discontinuous, and depend on climatic conditions; therefore, in their integration, renewable energy from these sources can cause security and stability problems in the electricity network.

Typically, the solar power has to be converted from its original Direct Current (DC) form to Alternating Current (AC) before it is supplied to the power grid or for other purposes. This conversion is crucial because most AC apparatuses and power grids operate on AC power. The primary device responsible for this conversion is an inverter, which has become a focal point of research and development efforts in recent years, as documented in multiple studies [2]–[12]. These studies explored various techniques and technologies for improving inverter efficiency and functionality, underscoring the importance of inverters in the broader context of PV energy utilization.

In several publications, the process of generating signals for the inverter has been carried out using different types of controller devices, each of which has unique features and capabilities. Specifically, the signal for the inverter was generated using PIC [4], [10], [11], ATMega 16 [9], Arduino [8], [13], and EG8010 [7] microcontrollers, whereas other devices were not explicitly mentioned [3], [5], [6]. Among these, a study published in [8] highlighted the use of an ATMega 328 microcontroller within a half-bridge topology to generate high-frequency signals in induction heater

applications. This approach demonstrates the versatility and adaptability of microcontrollers for optimizing the performance of inverters in various applications.

The control of a three-phase inverter is one of the most significant and traditional topics in power electronics, and it has been the subject of extensive research over the past few decades [14]. The importance of accurately controlling a three-phase inverter lies in its widespread use in various industrial and commercial applications where efficient and precise power conversion is essential. Numerous control systems have been developed to optimize the performance and reliability of inverters, reflecting ongoing advancements in power electronics technology.

Several control strategies have been proposed and implemented for three-phase inverters encompassing both nonlinear and linear approaches. Nonlinear methods, such as hysteresis control, offer dynamic and robust performance under various load conditions [2]. In contrast, linear techniques provide structured and predictable control through methods such as proportional-integral controllers using Pulse-Width Modulation (PWM) [14], [15], dead-beat control [16], multiloop feedback control [17], repetitive-based controllers [18], and sliding mode control [19]. Each of these techniques presents distinct advantages and is chosen based on the specific requirements of the application, highlighting the diverse approaches available for achieving an effective inverter control.

Previous research on inverter control using model predictive control was conducted in [20] using a robust disturbance observer to control the current output of a grid-connected inverter. The authors in [21] proposed a new maximum power point tracking method for PV modules based on Model Predictive Control (MPC) and a finite control set for model predictive current control of an inverter. Furthermore, in [22], a discrete-time model of the system is presented, able to predict the output voltage behavior for all possible switching states generated by the inverter.

Laguerre Model Predictive Control (LMPC) is a specialized form of MPC that employs the Laguerre function to enhance the optimization of its output. This approach leverages the unique properties of the Laguerre function to achieve a more precise control in various applications. Notably, this type of LMPC has been effectively implemented for managing load frequency control [23], buck-boost converters [24], mobile robots [25], autonomous vehicles [26], quadrotors [27], and vehicle platoons [28]. The successful application of the LMPC in these areas highlights its effectiveness in handling complex control tasks.

Prior research has not explored the application of LMPC for inverter control. This study introduces an LMPC algorithm designed to control a three-leg inverter connected to a three-phase grid system. This research aims to accomplish three main goals: 1) to develop an LMPC algorithm suitable for inverter applications, 2) to apply the algorithm for controlling the inverter, and 3) to evaluate the effectiveness of the proposed controller.

The structure of the paper is as follows: The problem formulations are outlined in Section 2. Section 3 presents and analyzes the simulation results using the LMPC algorithm in an inverter. The study concludes with Section 4.

II. PROBLEM FORMULATION

A. Inverter Model

Figure 1 depicts a three-phase inverter with an LC filter and unknown load. This model was used to present the mathematical relations.

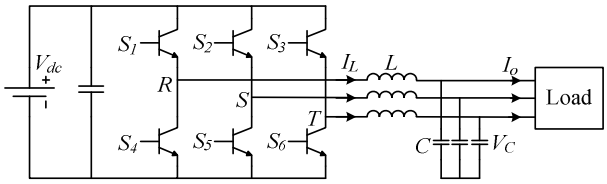

Fig. 1. Diagram of the test system.

Every leg of the inverter needs to have one switch turned on at all times to prevent the phases from shorting out. In fact, the switching states of S_R, S_S, and S_T are [10], [12], [17], [18], [22]:

$$S_R = \begin{cases} 1, \text{ if } S_1 = ON \text{ and } S_4 = OFF \\ 0, \text{ if } S_1 = OFF \text{ and } S_4 = ON \end{cases}$$

$$S_S = \begin{cases} 1, \text{ if } S_2 = ON \text{ and } S_5 = OFF \\ 0, \text{ if } S_2 = OFF \text{ and } S_5 = ON \end{cases} \quad (1)$$

$$S_T = \begin{cases} 1, \text{ if } S_3 = ON \text{ and } S_6 = OFF \\ 0, \text{ if } S_3 = OFF \text{ and } S_6 = ON \end{cases}$$

Since each leg of the inverter should have one switch turned on at all times, (1) is expressed as a vector of the switching states S as follows [10], [12], [17], [18], [22]:

$$S = \frac{2}{3}\left(S_R + \alpha S_S + \alpha^2 S_T\right) \quad (2)$$

Similarly, the inverter output voltage can be expressed as a vector and a function of the phase voltages:

$$V_i = \frac{2}{3}\left(V_{RN} + \alpha V_{SN} + \alpha^2 V_{TN}\right) \quad (3)$$

Where the phase voltages to ground are represented by V_{RN}, V_{SN}, and V_{TN} and $\alpha = 1\angle 120°$. The switching strategy of the inverter results in the development of distinct voltages at the input and output. Consequently, the inverter's output voltage vector can be considered as the constant input voltage multiplied by the switching vector or as follows [10], [12], [17], [18], [22]:

$$V_i = V_{dc} S \quad (4)$$

Where V_{dc} is the input's DC-link voltage. It can be inferred from (2) and (4) that the inverter produces eight output voltage vectors or switching states. The output voltages arising from the various switching states are displayed in Table I. Seven distinct voltage vectors were applied for every eight switching states, where V_0 equals V_7.

TABLE I. SWITCHING STATES

S_R	S_S	S_T	Voltage Vector
0	0	0	$V_0 = 0$
1	0	0	$V_1 = \frac{2}{3} V_{dc}$
1	1	0	$V_2 = \frac{1}{3} V_{dc} + j \frac{\sqrt{3}}{3} V_{dc}$
0	1	0	$V_3 = -\frac{1}{3} V_{dc} + j \frac{\sqrt{3}}{3} V_{dc}$
0	1	1	$V_4 = -\frac{2}{3} V_{dc}$
0	0	1	$V_5 = -\frac{1}{3} V_{dc} - j \frac{\sqrt{3}}{3} V_{dc}$
1	0	1	$V_6 = \frac{1}{3} V_{dc} - j \frac{\sqrt{3}}{3} V_{dc}$
1	1	1	$V_7 = 0$

Table I provides the main aspects of power electronics, specifically the relationship between the switching states in the inverter and the resulting output voltage vectors. The switching states represent the states of phases R, S, and T of the semiconductor devices in the circuit. The switches can either be "ON" or "OFF," denoted by 1 and 0. The sequence continues to cover all possible combinations of the three switches. The switches set out a symmetric pair with respect to the voltage vectors, including V_0 - V_7, V_1 – V_4, V_2 – V_3, and V_5 – V_6. These pairs are critical for balancing the three-phase output and minimizing harmonics in the output waveform. The complex vectors in the pair of V_2 – V_3, and V_5 – V_6 allow an imaginary unit that represents a 90°-phase shift at the output voltage.

B. Load Model

When modulation techniques are used, the inverter is regarded as a continuous form. Similarly, using (2) and (3), it is possible to define the load current I_o, output voltage (across the filter) V_c, and current flowing through the filter I_L as both a spatial vector and a unit relation based on three phases [10, 12, 17, 18, 22].

$$I_L = \frac{2}{3}\left(I_{LR} + \alpha I_{LS} + \alpha^2 I_{LT}\right) \quad (5)$$

$$I_o = \frac{2}{3}\left(I_{oR} + \alpha I_{oS} + \alpha^2 I_{oT}\right) \quad (6)$$

$$V_c = \frac{2}{3}\left(V_{cR} + \alpha V_{cS} + \alpha^2 V_{cT}\right) \quad (7)$$

Equations that are commonly used for predicting the output voltage are generated by computing the spatial vectors associated with each circuit parameter. Based on Figure 1, equations (8) and (9) are obtained using Kirchoff's law of voltage and current:

$$L\frac{dI_L}{dt} = V_i - V_c \quad (8)$$

$$C\frac{dV_c}{dt} = I_L - I_o \quad (9)$$

In state space, (8) and (9) can be written as follows [22]:

$$\begin{bmatrix} \dot{I}_L \\ \dot{V}_c \end{bmatrix} = \begin{bmatrix} 0 & -\frac{1}{L} \\ \frac{1}{C} & 0 \end{bmatrix} \begin{bmatrix} I_L \\ V_c \end{bmatrix} + \begin{bmatrix} \frac{1}{L} & 0 \\ 0 & -\frac{1}{C} \end{bmatrix} \begin{bmatrix} V_i \\ I_o \end{bmatrix} \quad (10)$$

$$y = \begin{bmatrix} 0 & 1 \end{bmatrix} \begin{bmatrix} I_L \\ V_C \end{bmatrix} \quad (11)$$

Equation (10) is regarded as the ultimate relationship and is used to predict the output voltage.

C. Discrete-Time Model for Prediction

Most of MPC is running in discrete time. Therefore, it is necessary to provide discrete equation (10) for the sampling period T_s to predict the output voltage. The discretization model is provided in (13) and (14). Then the discrete form of the inverter model in (10) is given in (12) as follows [22]:

$$x(k+1) = A_d x(k) + B_d u(k) + B_{dq} I_o(k) \quad (12)$$

$$A_d = e^{AT_s} \quad (13)$$

$$B_d = \int_0^{T_s} e^{A\tau} B d\tau \quad (14)$$

The predicted output voltage of the inverter V_i can be determined using (12). This formula uses measurements to determine the voltage and current of the filter, respectively, and specifies V_i in accordance with Table I and (4). Given that the load is regarded as uncertain, the following relation can be used to approximately determine I_o [22]:

$$I_o(k-1) = I_L(k-1) - \frac{C}{T_s}\left[V_c(k) - V_c(k-1)\right] \quad (15)$$

D. MPC Controller

An MPC is a multivariable, iteration-based control algorithm that counts the number of optimal control moves over its prediction horizon by utilizing an objective function, a process model, and past control moves. Under certain conditions, the objective function must not overcome any of the system's specified limitations. MPC is classified as a digital or continuous MPC based on signal processing, which can be linear or nonlinear depending on the internal model used [21], [23], [29], [30]. MPC finds the best solution in the prediction horizon H_p with the control horizon H_c, where $H_c \leq H_p$ at all times. MPC estimates the variable of interest H_p numbers in any time sample and attempts to attain it using the control attempt H_c [22, 23, 29, 30].

Low-harmonic sinusoidal voltages are generated when the inverter is used with an output LC filter. It requires some skill to obtain the inverter's control to operate in an appropriate switching state. A systemic model of the inverter with a finite number of switching states can be used to easily apply MPC [30]. One advantage of MPC voltage management is that it does not require load information, irrespective of the type of load, and a 50 Hz sinusoidal output voltage is produced.

A flawless trajectory model was used to design a predictive control system [22]. In fact, the cost function J, whose goal is

to have the output follow the intended value, is determined by the difference between the value produced by the MPC and the desired value of the variable.

The alpha-beta transformation employs the chosen cost function *J*, which is calculated by subtracting the reference voltage from the anticipated voltage. A sinusoidal voltage with a frequency of 50 Hz was used as the reference voltage. The voltage that minimizes the cost function and closely adheres to the reference value is considered ideal in this section, as follows [22]:

$$J = \left|V_{cr}^{ref} - V_{cr}^{p}\right| + \left|V_{ci}^{ref} - V_{ci}^{p}\right| \quad (16)$$

Where V^{p}_{cr} and V^{p}_{ci} denote the real and imaginary components of the output voltage V^{p}_{c}, respectively. Additionally, V^{ref}_{cr} and V^{ref}_{ci} represent the reference voltages V^{ref}_{c} for the real and imaginary parts, respectively.

E. Laguerre MPC Controller

The Laguerre function was used to define the model of the MPC controller, which used a model to estimate the behavior of the controlled plant. This function is an orthonormal function that can be used to construct the model, and it can also be used to simulate dynamic systems. This function was used to define the model of the MPC controller, which uses a model to forecast the behavior of a controlled plant. These characteristics are satisfied by Laguerre functions, which also exhibit straightforward Laplace transformations.

A continuous time framework is commonly utilized in the construction of a plant model. To be employed in discrete time MPC, the model must be discretized within a time sample. The Laguerre function, which is mostly used in the research of system identification, is primarily produced in continuous time by utilizing its network.

The Laguerre functions were obtained by inverting the z-transform of the Laguerre networks, as shown in (17). This function was formulated by following the dynamic model given in (18), where its initial condition is presented in (19). The parameters used in (17)-(19) are *N*, which is the Laguerre network's length, *a*, is the temporal scaling factor, A_l is a Toeplitz matrix of parameters *a* and 1-a^2, and *L* is the function's state vector [30].

$$\Gamma_N = \frac{\sqrt{1-a^2}}{1-az^{-1}}\left(\frac{z^{-1}-a}{1-az^{-1}}\right)^{N-1} \quad (17)$$

$$L(k+1) = A_l L(k) \quad (18)$$

$$L(0) = \sqrt{1-a^2}\left[1-a;\ \ a^2;\ \ -a^3;\ \ \ldots\ \ (-1)^{N-1}a^{N-1}\right] \quad (19)$$

Optimal receding horizon control is achieved by taking the minimal solution of an objective function J_c, as in (20).

$$J_c = \sum_{m=1}^{Np} x(k+m\,|\,k)^T Q x(k+m\,|\,k) + \eta^T R \eta \quad (20)$$

$$\eta = \left(\sum_{m=1}^{Np}\phi(m)Q\phi(m)^T + R_L\right)^{-1}\left(\sum_{m=1}^{Np}\phi(m)QA^m\right) \quad (21)$$

$$\phi(m) = \sum_{i=0}^{m} A^{m-i-1}BL(i)^T \quad (22)$$

Where *k* is the sampling instant, *m* is the prediction time, and $\eta \in \Re_{ns\,x\,N}$ is an optimal solution of the parameter vector. The future state variable estimated using the internal model is expressed as follows:

$$x(k+m\,|\,k) = A^m x(k) + \phi(m)^T \eta \quad (23)$$

Substituting (23) into (20), the objective becomes:

$$J_c = \eta^T\left(\sum_{m=1}^{Np}\phi(m)Q\phi(m)^T + R_L\right)\eta + 2\eta^T\left(\sum_{m=1}^{Np}\phi(m)QA^m\right)x(k) + \sum_{m=1}^{Np}x(k)^T(A^T)^m QA^m x(k) \quad (24)$$

The optimal solution to minimize J_c is given by:

$$J_c = \sum_{m=1}^{Np}x(k)^T(A^T)^m QA^m x(k) \quad (25)$$

Furthermore, the MPC gain K_{MPC} for the closed-loop system can be found in (27) [30].

$$x(k+1) = Ax(k) - BK_{MPC}u(k) \quad (26)$$

$$K_{MPC} = L(0)^T \eta \quad (27)$$

where A and B are the system matrices, RL is the rate of change in the control action weight matrix, and Q is the output error weight matrix.

F. Proposed Work

An MPC uses an objective function, process model, and previous control moves to count the number of optimum control moves over its prediction horizon. Under certain circumstances, the objective function cannot violate any of the stated restrictions on the system. Among the many advantages that MPC provides in process control are rapid reaction times, resistance to load variations, and parameter uncertainty [23].

Several prediction horizons can be considered to enhance system behavior, but doing so will increase system complexity and computational expense. Given the potential switching states of the converter, there can be a sizable number of alternative input sequences when a horizon length of H_p is employed. Thus, it is challenging to implement the concept of system behavior prediction for every potential switching state sequence in an actual system. Using H_p=1 is a straightforward method to reduce the number of calculations to the total number of switching states that the converter can have. Nonetheless, it is also possible to consider various prediction horizons to enhance system behavior, albeit at the expense of higher computational expense and system complexity.

The large number of prediction horizons will increase the MPC's complexity significantly. Applying these numbers to a system with fast dynamics when the machine hardware limits the computation might raise this issue. The use of the prediction horizon H_p=1 ≅ H_p>1 in certain special

circumstances of first-order systems, as shown analytically in [31].

The proposed controller is expected to be used in microcontrollers, Raspberry Pi, and other digital equipment. Therefore, simplification of the algorithm is useful for minimizing the processor's work. Based on this necessity, we decided to use the MPC's prediction horizon H_p=1, where the performance is comparable to a longer prediction horizon in a first-order system such as the inverter proved in [32]. Therefore, the flowchart of the proposed controller is given in Figure 2.

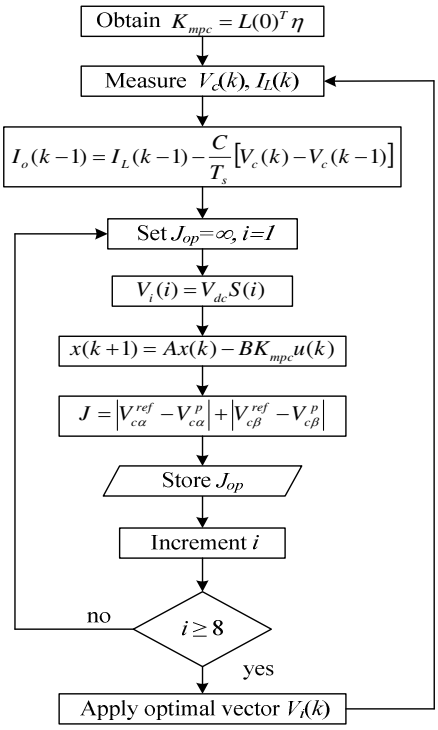

Fig. 2. Flowchart of the proposed controller.

The given LMPC algorithm can be expressed as a flow chart, as shown in Figure 2. The figure shows that the LMPC algorithm starts by obtaining the K_{MPC} gain. The step iteration is performed in the outer loop. At every step, the inverter applies a voltage vector to the length of the sample interval. The proposed predictive control uses information from measurements made at time k and accounts for the application of the new voltage vector in k+1 to create predictions up to time k+1. Some calculations are performed to determine the objective function based on the predictions of the output voltage V_i and the obtained output current I_o.

III. RESULTS AND DISCUSSION

A. Modelling and Controller Setting

The system for testing the proposed controller is consistent with a full-bridge IGBT MOSFET with an LC filter as structured in Figure 1. Several loads consisting of resistive (R), resistive-inductive (RL), and resistive-capacitive (RC) were applied to the inverter to test its performance. As expected, the frequency and amplitude of the voltage were adjusted to 50 and 500 V, respectively. In addition, the parameters used in the simulation were battery voltage V_{dc} = 850 VDC, reference voltage V_{ref} = 500 VAC, capacitor filter C_{filter} = 9.49 μF, inductor filter L_{filter} = 2.4 mH, and sampling time T_s = 20 μs.

A discrete model of the inverter for testing the proposed controller on a time sampling of approximately 20 μs was built based on the given data. The model was constructed using (10) and extended using (12). The inverter model was planned to be driven by the proposed LMPC. Another classical method using Sinusoidal Pulse Width Modulation (SPWM) was provided as a reference for comparing the effectiveness of the proposed controller. Both controllers operated at a frequency carrier of 1500 MHz, where the output frequency was 50 Hz.

The controller objective for the inverter application was to control the output voltage such that it meets the reference voltage while maintaining the output frequency constant at 50 Hz. To do so, some parameters of the LMPC controller were set: gain K_{MPC} = -0.9484, time scaling factor a = 0.3, network length N = 4, prediction, and control horizon $H_p = H_c = 1$.

B. Resistive Loads

In this simulation, the inverter was tested by placing a pure resistive (R) load of 4 kW at the output. The time interval for this test was 20 μs; therefore, the total simulation time was 0.1 s. The simulation results of both voltage and current outputs are shown in Figure 3 using the SPWM and LMPC controls in the dotted and solid lines, respectively. The Total Harmonic Distortions (THD) were measured and are presented in Table II.

TABLE II. THD RESULTS

Load Type	% Voltage THD			% Current THD		
	V_R	V_S	V_T	I_R	I_S	I_T
SPWM						
R	3.35	4.27	3.28	2.92	4.01	3.95
RC	2.61	3.47	2.43	7.77	8.49	8.48
Motor	5.17	11.76	8.99	12.86	8.50	16.65
LMPC						
R	1.16	1.04	1.14	1.16	1.04	1.14
RC	0.92	1.30	1.20	0.95	1.34	1.23
Motor	1.46	1.35	1.43	6.99	6.73	7.18

The maximum allowable current THD according to the IEEE 519-1992 standard is approximately 15%, whereas the voltage THD must not exceed 5% [33]. This standard was revised to the IEEE 519-2014 revision, where the acceptable THD of the current is 5% for small applications, while the voltage THD is increased for lower voltage applications of less than 1 kV to 8% [33]. Both the THD of the current and the voltage of the inverter were investigated using the revised IEEE 519-2014 standard. Figure 3 shows the inverter output when a resistive load is applied. The SPWM control results show a fairly smooth output voltage with a stable frequency of 50 Hz. On the other hand, the current produced was also sinusoidal, with a maximum magnitude of 4.63 A, although there were slight visible defects in the waveform. The distortion, which has an impact on the output wave defects, is

presented in Table II. It can be seen that the maximum THD for the voltage wave was 4.27%, and 4.01% for the current wave. Thus, the voltage and current THD do not exceed the maximum allowable values of 8% and 5%, respectively, according to the IEEE 519-2014 standard.

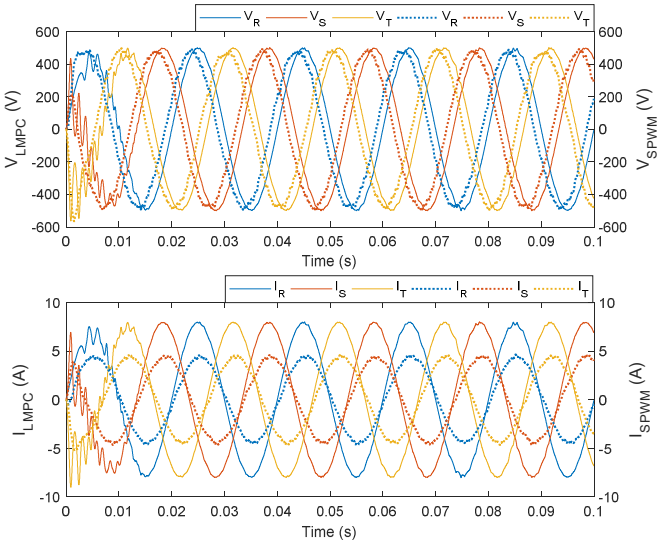

Fig. 3. SPWM (dot) and LMPC (solid) responses under R loads.

In contrast to SPWM, LMPC control provides better output results by setting the prediction horizon and control horizon to 1 each, as plotted in Figure 3. It can be observed that the inverter output voltage and current waves are smoother than those of the SPWM method. This can be validated by the resulting THDs, which have maximum values of 1.16% for both voltage and current. The action of the controller is shown in the first half waves of both the current and voltage outputs, which are very noisy. This differs from the SPWM method, which is an open-loop control method. On the other hand, the LMPC controller can provide a higher output current of up to 8.01 A, so the load is well supported. Owing to the characteristics of the resistive load R, which consumes electrical energy, the effect of the R load on the inverter output wave of both controllers might be seen in the increase in the current waveform. In this case, the R load changes the waveform but does not cause a shift in the current or voltage phase [20], [22].

C. Capacitive Loads

In this scenario, resistive and capacitive (RC) loads of 4 kW and 1 kW, respectively, were attached to the inverter. The simulation results obtained using the SPWM method and the LMPC controllers are shown in Figure 4. This simulation results from using the SPWM method with an almost perfect voltage output wave. However, there was a considerable distortion in the current output wave. The THD measurement results showed that the maximum current THD reached 8.49%, whereas the voltage THD was below 5%, with a maximum value of 3.47%. The THD of the current is just above the upper limit of the IEEE 519-2014 standard. The maximum current generated increased to approximately 5.52 A due to the RC load.

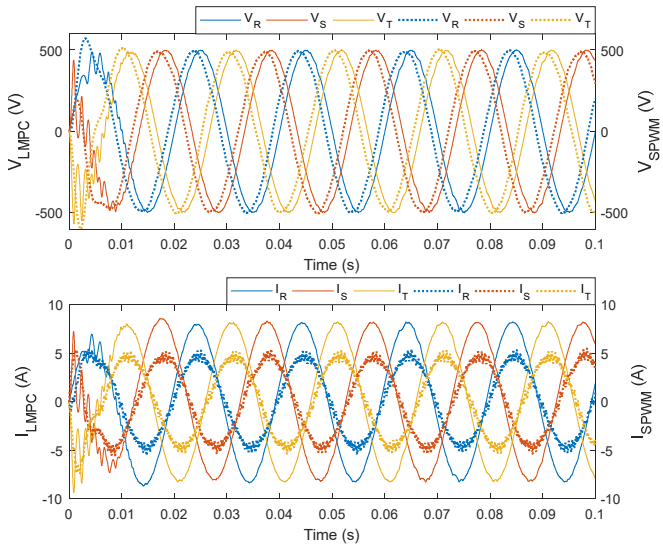

Fig. 4. SPWM (dot) and LMPC (solid) responses under RC loads.

Figure 4 also shows the simulation results with the LMPC controller with almost perfect voltage and current output waves, where the current waves reach 8.59 A. There was a higher distortion in the output current waveform, with a maximum value of 1.34%. Although initially, when the load was applied, the controller experienced a slightly large transient at 8% of the maximum time, later this condition could be immediately controlled so that the current THD could be better.

The effect of the RC load on the harmonic waves from both controllers reduced the voltage THD value on the inverter output wave. However, this type of load does not reduce the current THD value because the RC load only cuts off the voltage wave ripple [8], [20], [22].

D. Induction Motor Loads

In the final simulation, a 4 HP induction motor with an input torque of approximately 0.5 Nm was applied. The simulation results are shown in Figure 5 using both SPWM and LMPC control, as well as the measured THD, as presented in Table II.

As shown in Figure 5, when the induction motor load was loaded, there was a voltage drop of up to 294 V. Even though it did not reach its steady state throughout the simulation time, it showed an increase. However, the current response was quite high and then decreased throughout the simulation time from 32.11 A to 16.29 A. In this simulation, the voltage distortion was very high, reaching 16.65% and 15.17% for the THDs of current and voltage, respectively. This distortion implies that the SPWM output does not satisfy the IEEE 519-2014 standards, where the current and voltage THDs should not exceed 8% and 5%, respectively.

Similar to the SPWM voltage response, the LMPC response also experiences a voltage drop when starting the motor, but the LMPC is more aggressive in solving the drop, resulting in it reaching its steady state faster. The current response of the LMPC control shows a significant decrease in current from the

start to the end of the simulation, from 74.83 A to 8.68 A. As a result of the controller's aggressiveness, there is quite a lot of distortion in the initial period. Furthermore, after a period of 0.06s, the system reached a steady-state condition. Then, the distortion was greatly reduced in both the THDs of voltage and current, reaching 1.46% and 7.18%, respectively.

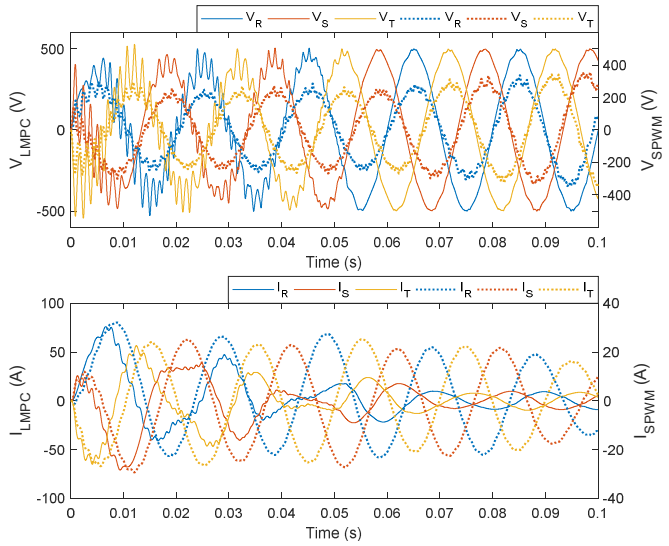

Fig. 5. SPWM (dot) and LMPC (solid) responses under motor loads.

Typically, the induction motor load represents an inductive load, where the harmonic waves reduce the current THD of the inverter output wave. However, this load type does not reduce the voltage THD, because the inductive load only cuts the current wave ripple. These conditions are visible in the simulation results, which show that the voltage ripple is higher for both controllers, which results in a high-voltage THD compared to the other load types [17], [18], [20], [22].

E. Performance Evaluation

Overall, based on simulations carried out for the combination of R, RC, and induction motor loads, the results show that the LMPC controller provides more satisfactory results than the classical SPWM controller. This evidence is proved by the controller's ability to generate greater output power following changes in load while maintaining the output voltage to meet the reference.

Furthermore, the generated distortion did not violated the IEEE 519-2014 standard, where the distortion exceeded 1.5% THD of the voltage. Although the THD of the current is higher for motor loads, it does not reach the minimum standard. The maximum current and voltage THDs recorded with the LMPC controller were 1.46% and 7.18%, respectively, all of which were achieved using induction motor loads.

IV. CONCLUSIONS

In this paper, a new inverter control strategy based on the optimal control of the Laguerre Model Predictive Control (LMPC) is presented. The proposed controller was tested on an inverter under various resistive (R), resistive-capacitive (RC), and induction motor loads at constant frequency and voltage. The controller performance was compared with that of a Sinusoidal Pulse-Width Modulation (SPWM) controller.

The simulation results show that the proposed LMPC controller has better advantages in meeting the reference voltage while providing quality voltage and current with low distortion of less than 1.5% and 8.0%, respectively, at various loads. The maximum Total Harmonic Distortion (THD) of the voltage and current of the LMPC controller were 1.46% and 7.18%, respectively, for the induction motor loads. Both the current and voltage THDs complied with the IEEE 519-2014 standard for harmonic distortion. Moreover, the proposed inverter provided a higher current output for each installed load than the SPWM controller. Therefore, LMPC is effective for controlling an inverter.

Although the simulations showed promising results, future research should focus on implementing the LMPC algorithm on a physical inverter system. This will provide valuable insights into the robustness, computational efficiency, and practical applicability of the algorithm.

ACKNOWLEDGMENTS

The authors thank the Indonesian Ministry of Education, Culture, Research, and Technology for funding this work under the scheme of "Penelitian Fundamental Reguler" with contract ID 076/E5/PG.02.00.PL/2024.

REFERENCES

[1] A. Rehiara, S. Setiawidayat, L. F. Marini, and S. Raharjo, "The Indonesian Government's Role in Setting Renewable Energy Targets to Reduce GHG Emissions from the Electrical Energy Sector," *Nakhara : Journal of Environmental Design and Planning*, vol. 22, no. 2, Nov. 2023, Art. no. 310, https://doi.org/10.54028/NJ202322310.

[2] A. E. Gadari, H. E. Ouardi, Y. Ounejjar, and K. Al-haddad, "Hysteresis control of the new split-packed-U-cell inverter," *Indonesian Journal of Electrical Engineering and Computer Science*, vol. 28, no. 3, pp. 1345–1354, Dec. 2022, https://doi.org/10.11591/ijeecs.v28.i3.pp1345-1354.

[3] N. Ahmed and Z. R. Khan, "Microcontroller Based Pure Sine Wave Inverter," in *2021 IEEE International Conference in Power Engineering Application*, Malaysia, Mar. 2021, pp. 173–177, https://doi.org/10.1109/ICPEA51500.2021.9417841.

[4] W. T. Hsu, Q. A. Liu, C. W. Huang, and Q. J. Xiao, "Design of Soft-Switching Inverter Power Supply Based on PWM in the Microcontroller," in *2020 International Conference on Wireless Communications and Smart Grid*, Qingdao, China, Jun. 2020, pp. 215–220, https://doi.org/10.1109/ICWCSG50807.2020.00055.

[5] S. A. Zulkifli, M. F. M. F. Tan, and M. J. M. Yusof, "Study on Power Converters Control in Hardware System Using Low Cost Microcontroller," in *2020 IEEE Student Conference on Research and Development*, Batu Pahat, Malaysia, Sep. 2020, pp. 1–4, https://doi.org/10.1109/SCOReD50371.2020.9251039.

[6] M. T. Richardson, V. Patterson, and A. Parchment, "Microcontroller Based Space Vector Pulse Width Modulation Speed Control of Three-phase Induction Motor," in *SoutheastCon 2021*, Atlanta, GA, USA, Mar. 2021, pp. 1–6, https://doi.org/10.1109/SoutheastCon45413.2021.9401922.

[7] K. Brahmana, "Utilization of the EG8010 Microcontroller to Construct a Pure Sine Inverter Using the Single Phase Sinusoidal Inverter ASIC (Application Specific Integrated Circuit) Method," *Journal of Technomaterial Physics*, vol. 2, no. 2, pp. 75–84, Aug. 2020, https://doi.org/10.32734/jotp.v2i2.5359.

[8] A. E. T. Maamar, M. Helaimi, R. Taleb, and F. Chabni, "Design and Control of a Single-Phase Series Resonance Inverter using an Arduino

Microcontroller," in *2019 International Conference on Advanced Electrical Engineering)*, Algiers, Algeria, Nov. 2019, pp. 1–6, https://doi.org/10.1109/ICAEE47123.2019.9014782.

[9] D. Setiawan, I. Ishak, and M. A. Sembiring, "Control System for Adjusting the Brightness Level with PWM Technique Using Visual Net Microcontroller-Based," *Journal of Robotics and Control*, vol. 1, no. 4, pp. 102–108, Mar. 2020, https://doi.org/10.18196/jrc.1422.

[10] S. Shuvo, E. Hossain, and Z. R. Khan, "Fixed Point Implementation of Grid Tied Inverter in Digital Signal Processing Controller," *IEEE Access*, vol. 8, pp. 89215–89227, 2020, https://doi.org/10.1109/ACCESS.2020.2993985.

[11] Dr. J. Dalei, A. Bisoi, S. Kumar, and R. Kumar, "Performance Analysis of Single Phase Multilevel Inverter Using dsPIC30F2010 Microcontroller," in *2019 IEEE International Symposium on Smart Electronic Systems*, Rourkela, India, Dec. 2019, pp. 41–46, https://doi.org/10.1109/iSES47678.2019.00022.

[12] A. Brahmi, G. Chbirik, A. Abounada, and E. mahjoub Boufounas, "Design of SPWM control unit based on microcontroller for photovoltaic inverters," in *2020 1st International Conference on Innovative Research in Applied Science, Engineering and Technology*, Meknes, Morocco, Apr. 2020, pp. 1–5, https://doi.org/10.1109/IRASET48871.2020.9092054.

[13] D. Setiawan, H. Eteruddin, and A. Arlenny, "Desain dan Analisis Inverter Satu Fasa Berbasis Arduino Menggunakan Metode SPWM," *Jurnal Teknik*, vol. 13, no. 2, pp. 128–135, Oct. 2019, https://doi.org/10.31849/teknik.v13i2.3470.

[14] J. Rodriguez *et al.*, "Predictive Current Control of a Voltage Source Inverter," *IEEE Transactions on Industrial Electronics*, vol. 54, no. 1, pp. 495–503, Feb. 2007, https://doi.org/10.1109/TIE.2006.888802.

[15] H. Alam, M. Irwanto, Y. M. Mashor, and M. Masri, "Design of multiple Pulse Width Modulation (MPWM) Transformerless Photovoltaic Inverter (TPVI) system," *Journal of Physics: Conference Series*, vol. 1432, no. 1, Jan. 2020, Art. no. 012056, https://doi.org/10.1088/1742-6596/1432/1/012056.

[16] W. Yao, J. Cui, and W. Yao, "Single-Phase Inverter Deadbeat Control with One-Carrier-Period Lag," *Electronics*, vol. 9, no. 1, Jan. 2020, Art. no. 154, https://doi.org/10.3390/electronics9010154.

[17] S.-J. Yoon and K.-H. Kim, "Multiloop current control for an inductive–capacitive–inductive-filtered grid-connected inverter with frequency-adaptive capability under distorted grid environment," *IET Power Electronics*, vol. 12, no. 6, pp. 1521–1531, 2019, https://doi.org/10.1049/iet-pel.2018.6259.

[18] H. Zhang, Q. Zhao, S. Wang, and X. Yue, "Improved Repetitive Control for an LCL-Type Grid-Tied Inverter with Frequency Adaptive Capability in Microgrids," *Electronics*, vol. 12, no. 7, Jan. 2023, Art. no. 1736, https://doi.org/10.3390/electronics12071736.

[19] Q.-T. Tran, "An Application of Neural Network-based Sliding Mode Control for Multilevel Inverters," *Engineering, Technology & Applied Science Research*, vol. 14, no. 1, pp. 12530–12535, Feb. 2024, https://doi.org/10.48084/etasr.6516.

[20] N. N. Nam, M. Choi, and Y. Il Lee, "Model Predictive Control of a Grid-Connected Inverter with LCL Filter using Robust Disturbance Observer," *IFAC-PapersOnLine*, vol. 52, no. 4, pp. 135–140, Jan. 2019, https://doi.org/10.1016/j.ifacol.2019.08.168.

[21] Y. Zhao, A. An, Y. Xu, Q. Wang, and M. Wang, "Model predictive control of grid-connected PV power generation system considering optimal MPPT control of PV modules," *Protection and Control of Modern Power Systems*, vol. 6, Dec. 2021, Art. no. 32, https://doi.org/10.1186/s41601-021-00210-1.

[22] I. S. Mohamed, S. Zaid, M. F. A. Elyazeed, and H. Elsayed, "Implementation of model predictive control for three-phase inverter with output LC filter on eZdsp F28335 Kit using HIL simulation," *International Journal of Modeling, Identification and Control*, vol. 25, no. 4, pp. 301–312, 2016.

[23] A. B. Rehiara, N. Yorino, Y. Sasaki, and Y. Zoka, "A novel adaptive LFC based on MPC method," *IEEJ Transactions on Electrical and Electronic Engineering*, vol. 14, no. 8, pp. 1145–1152, 2019, https://doi.org/10.1002/tee.22912.

[24] A. B. Rehiara and Y. Rumengan, "Model Predictive Control Untuk Kendali Konverter Buck-Boost," *ReTII*, pp. 109–114, Oct. 2020.

[25] M. Jamalabadi, M. Naraghi, I. Sharifi, and E. Firouzmand, "Robust Laguerre based model predictive control of nonholonomic mobile robots under slip conditions," in *2021 7th International Conference on Control, Instrumentation and Automation*, Tabriz, Iran, Feb. 2021, pp. 1–5, https://doi.org/10.1109/ICCIA52082.2021.9403540.

[26] M. Elsisi, "Model Predictive Control with Laguerre Function based on Social Ski Driver Algorithm for Autonomous Vehicle," in *2020 International Conference on Advanced Robotics and Intelligent Systems*, Taipei, Taiwan, Aug. 2020, pp. 1–6, https://doi.org/10.1109/ARIS50834.2020.9205782.

[27] P. Sharma, U. Bajpai, S. Kumar Saha, and A. Jawed, "Constrained Control of Quadrotor Using Laguerre Functions Based Model Predictive Control for Reference Tracking," in *Proceedings of the 2021 5th International Conference on Advances in Robotics*, Kanpur, India, Dec. 2022, pp. 1–7, https://doi.org/10.1145/3478586.3478604.

[28] R. Resmi, S. J. Mija, and J. Jacob, "Discrete Laguerre-based model predictive control for dynamic consensus of a vehicle platoon with time delay," *International Journal of Systems Science*, vol. 53, no. 12, pp. 2566–2583, Sep. 2022, https://doi.org/10.1080/00207721.2022.2067911.

[29] A. B. Rehiara, H. Chongkai, Y. Sasaki, N. Yorino, and Y. Zoka, "An adaptive IMC-MPC controller for improving LFC performance," in *2017 IEEE Innovative Smart Grid Technologies - Asia*, Auckland, New Zealand, Dec. 2017, pp. 1–6, https://doi.org/10.1109/ISGT-Asia.2017.8378403.

[30] A. B. Rehiara, H. Chongkai, Y. Sasaki, N. Yorino, and Y. Zoka, "An Adaptive Internal Model for Load Frequency Control Using Extreme Learning Machine," *TELKOMNIKA (Telecommunication Computing Electronics and Control)*, vol. 16, no. 6, Dec. 2018, Art. no. 2879, https://doi.org/10.12928/telkomnika.v16i6.11553.

[31] J. Sawma, F. Khatounian, E. Monmasson, R. Ghosn, and L. Idkhajine, "The effect of prediction horizons in MPC for first order linear systems," in *2018 IEEE International Conference on Industrial Technology*, Lyon, France, Feb. 2018, pp. 316–321, https://doi.org/10.1109/ICIT.2018.8352196.

[32] R. Sutjipto, W. Kusuma, and K. Zulfianta, "Analisis Pengaruh Harmonisa Terhadap Losses Transformator 500kVA," *Elposys: Jurnal Sistem Kelistrikan*, vol. 9, no. 2, pp. 40–45, Jun. 2022, https://doi.org/10.33795/elposys.v9i2.614.

[33] "IEEE Recommended Practice and Requirements for Harmonic Control in Electric Power Systems," *IEEE Std 519-2014 (Revision of IEEE Std 519-1992)*, pp. 1–29, Jun. 2014, https://doi.org/10.1109/IEEESTD.2014.6826459.